Surface-Enhanced Vibrational Raman Optical Activity: A Time-Dependent Density Functional Theory Approach†

Lasse Jensen*

Department of Chemistry, The Pennsylvania State University, 104 Chemistry Building, University Park, Pennsylvania 16802

Received: December 15, 2008; Revised Manuscript Received: January 28, 2009

In this work we present the first simulations of the surface-enhanced Raman optical activity (SEROA) using time-dependent density functional theory (TDDFT). A consistent treatment of both the chemical and electromagnetic enhancements is achieved by employing a recently developed approach based on a short-time approximation for the Raman and ROA cross-sections. As an initial application we study a model system consisting of adenine interacting with a Ag_{20} cluster. Because both the silver cluster and adenine in the absorption geometry are achiral, the chiroptical properties are due to the interactions between the two systems. Our results show that the total enhancement is on the order of 10^4 both for SEROA and SERS. However, the chemical enhancement is found to be larger for SEROA than for SERS. The results presented here show that SEROA can be a useful approach for studying induced chirality in small metal clusters due to the absorption of molecules.

Introduction

By measuring the small difference in the Raman intensities due to right- and left-circularly polarized incident light, Raman optical activity (ROA) gives structural information related to the chirality of molecules. This makes the method uniquely suited for studying biomolecules because it does not rely on electronic resonances, can easily be performed in aqueous solution, and is sensitive to molecular chirality, thus providing detailed information about the secondary and tertiary structures of biomolecules in their native environment.[1−3] ROA has proved to be a valuable tool in biomolecular research, and its versatility is clearly illustrated by the large variety of systems that have been explored. This includes systems such as small molecules such as peptides and carbohydrates,[4−6] folded and unfolded proteins,[7−9] intact glycoproteins,[10] RNA and DNA,[11] and the nucleic acid components of intact viruses.[12] However, the method is hampered by the low signal intensities which are around a thousand times weaker than the already weak Raman intensities. Large ROA signals can be achieved in surface-enhanced Raman optical activity (SEROA) due to both a surface-enhanced Raman scattering (SERS)-like enhancement of the overall scattering and enhancements from a large electric field gradient at the metal surface.[13−21] SEROA is a unique technique because it combines the powerful structural information of ROA with the strong enhancements known for SERS. However, only a few experimental studies have been reported to date.[18−21]

While the theory for SERS is fairly advanced[22−26] much less is known about SEROA. Janesko and Scuseria devised a method to determine SEROA by combining the electromagnetic response of orientationally averaged model substrates with Raman optical activity expressions.[17] This model was based on the earlier electromagnetic theory of Efrima.[13,14] Bour later[27] reformulated this in matrix form and generalized it for multiple particles. These models treat the electromagnetic enhancements due to the nanoparticles; however, so far they have only been used for simple geometric particles. Efrima showed that in addition to enhancements from the local field due to plasmon excitations, a contribution from the electric field gradient at the surface would also result in an enhanced ROA signal. This was later confirmed by Janesko and Scuseria who did explicit calculations on a model system consisting of (*R*)-(−)-bromochlorofluoromethane interacting with either a dipolar or a quadupolar substrate. These electromagnetic theories predict that the enhancement of ROA could be larger than SERS for certain substrates, making SEROA and SERS comparable.[13,14,17,27]

The theoretical models of Efrima, Scuseria, and Bour have so far only considered the electromagnetic enhancements. However, from SERS it is well-known that there are two contributions resulting, respectively, from electromagnetic (EM) and chemical interactions (CHEM) between the adsorbate and the metal nanoparticle.[23,26,28,29] The local field and field gradient enhancements arising from the plasmon excitations can be very large and are currently believed to be the dominant contribution to the observed SEROA signal.[14,17] However, so far there has been no studies of the CHEM effect on SEROA.

In this article we present the first simulations of SEROA of adenine interacting with a small silver cluster using a new quantum chemistry method based on time-dependent density functional theory.[30] The simulated SERS spectra will also be presented and compared with experimental results. The method has previously been used to study SERS of pyridine interacting with small metal clusters.[26,31−33] Although limited to small metal clusters, this method provides a consistent treatment of both the EM and CHEM enhancement mechanisms and can be a useful approach for getting a microscopic understanding of SEROA. Adenine is interesting because it belongs to a large family of so-called prochiral molecules (although theory predicts adenine to be chiral in the gas phase). These molecules become chiral when adsorbed on a surface, and little is known about their chiroptical properties when adsorbed. Our results show that the total enhancement is on the order of 10^4 both for SEROA and for SERS.

† Part of the "George C. Schatz Festschrift" Special Issue.

* Corresponding author. E-mail: jensen@chem.psu.edu.

10.1021/jp811084x CCC: $40.75
Published on Web 03/16/2009

However, the CHEM enhancement is found to be larger for SEROA than for SERS. While these methods cannot provide a complete picture of SEROA, because they are limited to rather small metal clusters, they provide the detailed description necessary for constructing more realistic models that can treat large metal nanoparticles.

Theory

Raman and ROA measurements can be performed using different experimental setups, each leading to a different relation between the measured intensities and the molecular properties. In a backscattering geometry the Raman intensites are given by[34−36]

$$I^{R}(180°) + I^{L}(180°) = \frac{d\sigma}{d\Omega}(180°) = K_p\left[\frac{90\alpha_p^2 + 14\beta(\alpha)_p^2}{90}\right] \quad (1)$$

where $\alpha_p$and $\beta(\alpha)_p^2$ are the isotropic and anisotropic invariants of the dipole−dipole polarizability transition tensor. The parameter K_p, which is independent of the experimental setup but depends on both the incident and scattered frequencies, is given by

$$K_p = \frac{\pi^2}{\varepsilon_0^2}(\tilde{\nu}_{in} - \tilde{\nu}_p)^4 \frac{h}{8\pi^2 c\tilde{\nu}_p} \frac{1}{1 - \exp[-hc\tilde{\nu}_p/k_B T]} \quad (2)$$

where $\tilde{\nu}_{in}$and $\tilde{\nu}_p$ are the frequencies of the incident light and of the pth vibrational mode, respectively. The corresponding ROA intensities are then given by[34−36]

$$I^{R}(180°) - I^{L}(180°) = \Delta\frac{d\sigma}{d\Omega}(180°) = K_p\left[\frac{48(\beta(G')_p^2 + \beta(A)_p^2/3)}{90c}\right] \quad (3)$$

where c is the speed of light, $\beta(G')_p$ the anisotropic invariant of the product of the electric dipole−magnetic dipole polarizability transition tensor and the electric dipole−dipole polarizability transition tensor, and $\beta(A)_p$ the anisotropic invariant of the product of the electric dipole−electric quadrupole polarizability transition tensor with the electric dipole−dipole polarizability transition tensor. The different invariants contributing to the Raman and ROA intensities consist of tensor contractions of different combinations of the dipole−dipole polarizability transition tensor, $\alpha^p_{\alpha\alpha}$, the electric dipole−magnetic dipole polarizability transition tensor, $G'^p_{\alpha\beta}$, and the electric dipole−electric quadrupole polarizability transition tensor, $A^p_{\gamma,\delta\beta}$.

In order to calculate the polarizability transition tensors, one typically adopts the Placzek approximation which is in general valid in the off-resonance case. However, by adopting a short-time approximation one can formulate a Placzek-like polarizability theory which is valid both on- and off-resonance.[37−42] Within the Placzek-like approximation, the transition tensors are expanded in a Taylor series around the equilibrium geometry. The transition tensors can then be expressed as geometric derivatives of molecular properties as

$$\alpha^p_{\alpha\beta}\alpha^p_{\alpha\beta} = \langle 0|\alpha_{\alpha\beta}|1_p\rangle\langle 1_p|\alpha_{\alpha\beta}|0\rangle = \left(\frac{\partial\alpha_{\alpha\beta}}{\partial Q_p}\right)_0\left(\frac{\partial\alpha_{\alpha\beta}}{\partial Q_p}\right)_0 \quad (4)$$

$$\alpha^p_{\alpha\beta}G'^p_{\alpha\beta} = \langle 0|\alpha_{\alpha\beta}|1_p\rangle\langle 1_p|G'\alpha\beta|0\rangle = \left(\frac{\partial\alpha_{\alpha\beta}}{\partial Q_p}\right)_0\left(\frac{\partial G'\alpha\beta}{\partial Q_p}\right)_0 \quad (5)$$

$$\alpha^p_{\alpha\beta}\varepsilon_{\alpha\gamma\delta}A^p_{\gamma\delta\beta} = \langle 0|\alpha_{\alpha\beta}|1_p\rangle\langle 1_p|\varepsilon_{\alpha\gamma\delta}A_{\gamma,\delta\beta}|0\rangle = \left(\frac{\partial\alpha_{\alpha\beta}}{\partial Q_p}\right)_0\varepsilon_{\alpha\gamma\delta}\left(\frac{\partial A_{\gamma,\delta\beta}}{\partial Q_p}\right)_0 \quad (6)$$

where Q_p is the normal mode of the pth vibration, $\alpha_{\alpha\beta}$ the electric dipole−dipole polarizability, $G'_{\alpha\beta}$ the electric dipole−magnetic dipole polarizability, and $A_{\gamma\delta\beta}$ the electric dipole−quadrupole polarizability. In the short-time approximation, the molecular properties are complex.

We have recently presented an approach to calculate the different generalized polarizability tensors needed for ROA both on- and off-resonance by including the finite lifetime of the electronic excited states.[43−47] This finite lifetime is included phenomenologically by a common damping parameter Γ,[48−51] which describes relaxation and dephasing of the excited state. The incorporation of a damping into the polarizability calculations has been described previously, and readers are referred to ref 43−47 for details. Here, this approach is combined with numerical differentiation to calculate the generalized polarizability derivatives needed to obtain the ROA scattering intensities. Gauge independent results are obtained by adopting the modified velocity gauge (MVG) form for calculating the response functions.[46,47,52]

Computation Details

All calculations presented in this work were performed using a local version of the Amsterdam Density Functional (ADF) program package.[53,54] The Becke−Perdew (BP86) XC-potential[55,56] and a triple-ζ polarized slater type (TZP) basis set from the ADF basis set library were used. The 1s-3d core was kept frozen for Ag, and all cluster-molecule complexes used frozen 1s cores for C, N, and O. Scalar relativistic effects were accounted for by means of the zeroth-order regular approximation (ZORA).[57,58] The vibrational frequencies and normal modes were calculated within the harmonic approximation, and for this reason the BP86 functional was chosen because it usually gives harmonic frequencies close to experimental results without the use of scaling factors.[59] Additionally, all Ag atoms were frozen in the vibrational frequency calculations to reduce the computational time. The cluster geometry chosen was taken from the work of Doye and Wales.[60] This structure was found to be the global minima using the Sutton−Chen potentials.

The calculations of the generalized polarizabilities and generalized polarizability derivatives were performed using the AORESPONSE module[42−47,61] of the ADF program package.[53,54] The calculations of the polarizability derivatives were carried out using a numerical three-point differentiation with respect to Cartesian displacements. A damping parameter in the range of $\Gamma \sim 0.0037-0.008$ a.u. (800−1600 cm^{-1}) is what we have found previously to be reasonable, and for all the results presented in the following, a value $\Gamma = 0.0037$ a.u. was used unless otherwise stated. However, one should be aware of the fact that the resonance SERS and SEROA intensites roughly

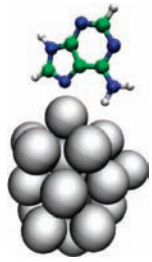

Figure 1. Configuration of the adenine−Ag_{20} complex. The figure was prepared using VMD.[70]

scale as $1/\Gamma^4$, and therefore the calculated enhancement factors on resonance depend strongly on Γ.[26,62,63] The vibrational circular dichroism (VCD) spectra were calculated using the recent implementation by Nicu et al.[64] Atomic units are used unless otherwise stated.

Results

SERS of adenine has been studied experimentally by Giese and McNaughton,[65] and the normal modes were assigned by comparison with DFT calculations. They find that adenine on silver colloids binds predominantly through one of the nitrogens in an almost perpendicular orientation. Here we will adopt this configuration and an illustration of the adenine structure, and its orientation relative to a silver cluster is shown in Figure 1. In the following sections we will present the bonding properties of the adenine−Ag_{20} complex, the ultraviolet−visible (UV−vis) absorption and electronic circular dichroism (CD) of the complex, the Raman, vibrational circular dichroism (VCD), and ROA spectra of adenine, the surface-enhanced VCD (SEVCD) of the complex, and SERS and SEROA spectra of the complex at two different incident wavelengths. While the UV−vis absorption and electronic CD spectra mainly reflect the silver core, the vibrational spectroscopies (VCD, Raman, and ROA) provide information about the molecules absorbed on the silver cluster. This has recently been demonstrated for small monolayer-protected gold clusters where VCD has been used to probe directly the structure of chiral adsorbed molecules.[66−68]

It is well established that adenine in the gas phase is slightly nonplanar with the two hydrogen on the amino group to be out of the ring plane.[65,69] This means that it is in principle possible to measure the chiral response of the free molecule in the gas phase, although such a measurement would be very difficult in practice due to the small energy difference between the two structures. In addition, adenine is planar in DNA due to its interactions with the surroundings. This is also confirmed here where adenine becomes planar upon interacting with the achiral silver cluster. Therefore, the interactions between the two achiral species form a chiral complex due to the breaking of the mirror plane in both molecules, and the chiroptical response is best interpreted as arising from the interactions with the metal cluster. However, we will present the chiroptical properties of the free nonplanar adenine in order to establish the enhancements of the chiral response due to the interactions with the metal cluster.

Bonding Properties. To understand the interactions between the two molecules we have analyzed the binding energy, the Ag−N bond length (R_{Ag-N}) and the charge transferred from adenine to Ag_{20} of the complex using the extended transition state method developed by Ziegler and Rauk.[71−74] The interaction energy can be decomposed into three physical contributions as[74] $\Delta E = \Delta E^{el} + \Delta E^{Pauli} + \Delta E^{orb}$. The first term is the classical electrostatic interaction between the unperturbed charge distributions of the two fragments, the second term is the Pauli repulsion which represents the destabilization due to interaction between occupied orbitals and accounts for steric repulsion, and the last term is the interaction between occupied and virtual orbitals and accounts for electron pair bond formation, charge transfer, and polarization.[54] We neglect the preparation energy, i.e., the energy needed to deform the isolated fragments to their structures in the complex, and the basis set superposition errors because they were found previously to be rather small (<1 kcal mol^{-1}) for similar systems.[31] We find the bonding energy for adenine interacting with the silver cluster to be $\Delta E = -16.8$ kcal/mol with a bond length of R_{Ag-N}=2.247Å. The largest contribution to the bonding energy is from $\Delta E^{orb} = -26.21$ kcal/mol, and the sum of the electrostatic and Pauli repulsion is destabilizing by 9.41 kcal/mol. The amount of charge transferred from adenine to the silver cluster was found to be 0.132e using the Voronoi deformation density (VDD) charges.[54] Both the interaction energy and the charge transferred are very similar to what we found previously for pyridine interacting with small silver clusters and is typical of physisorption or weak chemisorption.[31,33] Therefore, we would expect the interaction between adenine and the silver cluster to result in similar enhancements of the Raman cross-sections as we have found previously for pyridine.

UV−vis Absorption and Electronic Circular Dichroism of Adenine−Ag_{20}. To simulate the absorption and CD spectra of the complex, we calculated all electronic transitions as well as the oscillator strengths and rotatory strengths up to 3.8 eV. The simulated absorption and CD spectra of the complex are displayed in Figure 2. We see that the absorption spectrum is characterized by a strong band around 344 nm. This band corresponds to a large collection of individual excitations and can be thought of as a microscopic analogue to the strong plasmon resonances found in larger metal nanoparticles. Because the isolated metal cluster is achiral and the adenine becomes planar upon absorption the CD spectrum is induced by the complexation. The CD spectrum shows a negative band around 344 nm and a positive band around 400 nm. The CD spectrum is the result of a large number of excitations with both positive and negative rotatory strengths and therefore is expected to be very sensitive to the interactions between adenine and the silver cluster. Such a large induced CD has been observed experimentally in small (<3 nm) chiral monolayer protected clusters consisting of a gold core and a glutathione adsorbate layer.[75] It has been shown that the chiral response can result from a dissymmetric perturbation of the symmetric metal core by the chiral adsorbate.[76] However, in our case both the adsorbate and the metal cluster are achiral, and the chiral response is a result of the interactions.

Raman, ROA, and VCD Spectra of Adenine. Before studying the surface-ehancement of adenine due to interactions with the silver cluster, we first simulate the Raman and ROA spectra of adenine at an incident wavelength of 514.5 nm and the VCD spectra. The simulated Raman, ROA, and VCD spectra of adenine are presented in Figure 3a, Figure 3b, and Figure 3c, respectively. Experimentally, the Raman spectrum of polycrystalline adenine is dominated by strong bands at 1483, 1333, and 723 cm^{-1}, with the band at 723 cm^{-1} being the strongest.[65] In the simulated Raman spectrum, we find the strongest peaks to be at 1462/1451, 1330/1315, and 706 cm^{-1}. Overall there is a fair agreement between the experimental spectra and the one we calculated. One exception is the band at 706 cm^{-1} corresponding to the strongest band at 723 cm^{-1} in the experiments, for which the intensity is severely underestimated in the simulation. A recent theoretical study has shown that using new range-separated hybrid functionals can lead to a better agreement

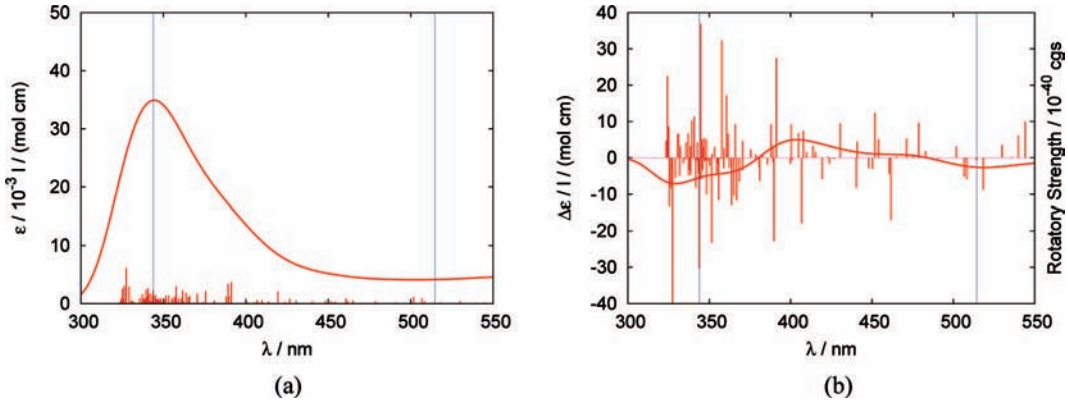

Figure 2. Simulated (a) UV−vis absorption and (b) CD spectra of adenine interacting with a Ag_{20} cluster in two different configurations.

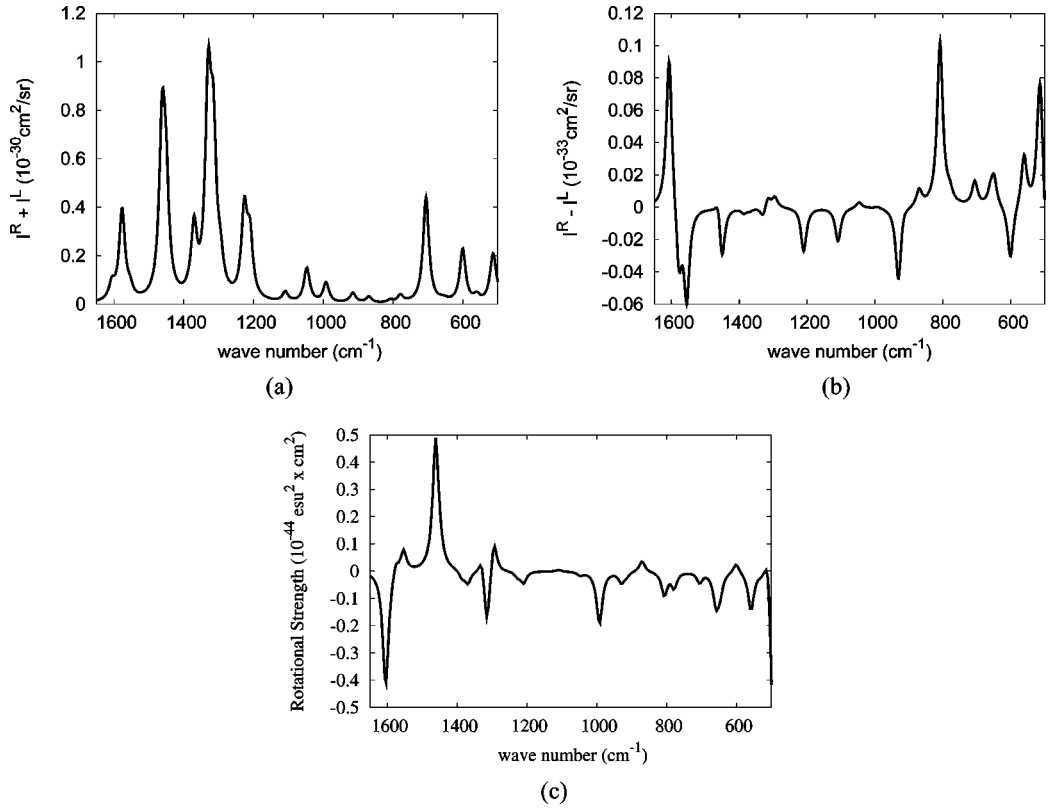

Figure 3. Simulated (a) Raman, (b) ROA for adenine at an incident wavelength of 514.5 nm, and (c) VCD. The Raman and ROA spectra are in units of 10^{-30} cm^2/sr and 10^{-33} cm^2/sr, respectively, and the VCD in units of 10^{-44} esu^2 × cm^2. All simulated spectra have been broadened with a Lorentzian having a full width at half-maximum (fwhm) of 20 cm^{-1}.

with experiments, although the relative intensity of the band around 700 cm^{-1} is still underestimated.[77] However, the experimental Raman spectrum is for polycrystalline adenine and thus should show interactions between different adenine molecules. Therefore, it would be of interest to examine if part of the discrepancy between theory and experiments stems from adenine−adenine interactions.

The ROA spectrum is dominated by a positive−negative doublet around 1600 cm^{-1} and a positive band around 800 cm^{-1}. We see that the ROA signal is 10^3 times weaker than that of the corresponding Raman spectra. The ratio of the ROA intensities and Raman intensities are expressed in terms of the dimensionless circular intensity differences (CID) as

$$\Delta = \frac{I^{\mathrm{R}} - I^{\mathrm{L}}}{I^{\mathrm{R}} + I^{\mathrm{L}}} \tag{7}$$

We calculated the average CID $\langle\Delta\rangle$ for the modes in the spectrum region between 500−1800 cm^{-1}, thus reflecting the average intensity difference between the Raman and the ROA signal. For adenine we obtained $\langle\Delta\rangle \sim 0.78 \times 10^{-3}$ which are in good agreement with the expectation that ROA is about a 1/1000 times weaker than Raman. Also, it is important to note that the bands that are strong in the Raman spectrum are not necessarily strong in the ROA spectrum, illustrating that ROA provides complimentary structural information. The fact that the spectrum consists of both positive and negative bands makes ROA particular sensitive to even small changes in the structure and therefore an attractive technique for probing the structures of biomolecules. This is also the case for VCD where the spectrum of adenine (Figure 3c) is dominated by one negative peak at 1605 cm^{-1} and a positive peak at 1462 cm^{-1}. Also, the spectral signature of VCD is significantly different than ROA making the two techniques complimentary.

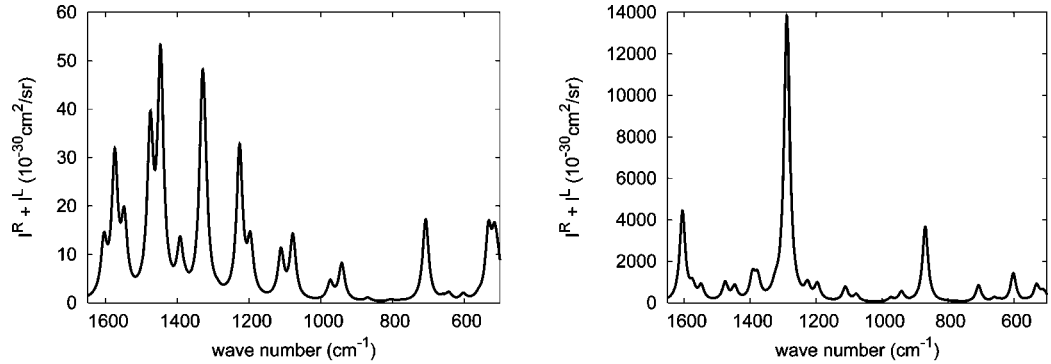

Figure 4. Simulated SERS spectra for adenine−Ag_{20} in units of 10^{-30} cm^2/sr at an incident wavelength of (a) 514.5 nm and (b) 344 nm, respectively. All simulated spectra have been broadened with a Lorentzian having a full width at half-maximum (fwhm) of 20 cm^{-1}.

SERS, SEVCD, and SEROA of Adenine−Ag_{20}. In this subsection, we present simulated surface enhanced Raman scattering (SERS), surface enhanced VCD, SEVCD, and surface enhanced Raman optical activity (SEROA) spectra of the adenine−Ag_{20} complex. The total enhancement can roughly be understood in terms of four mechanisms:[26] an electromagnetic mechanism (EM) due to resonance of the incident beam with the plasmon of the metal surface, a charge transfer (CT) mechanism due to resonance of the incident beam with an excitation from the metal to the adsorbate, a resonance mechanism where the incident beam is resonant with a molecular excitation, and an enhancement due to nonresonant interactions between the surface and the adsorbate (CHEM).[22,23,26] In the following, we only consider the nonresonant chemical and electromagnetic enhancement mechanisms. The enhancement in the Raman and ROA cross-section for the complex calculated at 514.5 nm relative to that for adenine in the absence of the cluster provides a direct measure of the CHEM enhancement, while the cross-section at the metal resonance wavelength (344 nm) provides an estimate of the combined chemical and electromagnetic enhancements. The enhancements found in SEVCD are similar in nature to the CHEM enhancement from SERS and SEROA. One should realize here that the cluster studied is too small to have a real plasmon resonance which involves a collective excitation of all of the conduction electrons. Instead the electronic excitations are molecular in character. However the excited-state can still give rise to the same type of enhancement effects that are familiar from SERS, so we use the same notation.

In Figure 4 we present the simulated SERS spectra for the adenine−Ag_{20} complex at incident wavelengths of 514.5 and 344 nm. The SERS spectrum simulated at 514.5 nm is off resonance with the strong silver transition, and the enhancement should therefore reflect the CHEM mechanism. However, at 344 nm the wavelength is resonant with the strong absorption band of the complex, and the enhancement should arise from a combination of the CHEM and the EM mechanisms. If we compare the SERS spectrum of the complex presented in Figure 4a with the Raman spectrum of adenine in Figure 3a, we see that the overall spectral appearance is similar although there are more strong bands in the region between 1600−1200 cm^{-1}. The Raman intensities are enhanced by about a factor of 50 when adenine is absorbed onto the metal cluster. This is higher than our previous results of pyridine interacting with a tetrahedral Ag_{20} cluster,[31,33] because of the different geometry of the metal cluster used in this work. Comparing the SERS spectrum calculated at 344 nm (Figure 4b) with the Raman spectrum of adenine (Figure 3a), we see that there is a significant change in both the relative intensities and the total cross-sections. The SERS spectrum is dominated by a strong band at 1288 cm^{-1} and two weaker bands at 1604 and 867 cm^{-1}. The overall enhancement is on the order of 10^4 compared with the Raman spectrum of adenine and 3×10^2 compared with the SERS spectrum of the complex calculated at 514.5 nm. Thus, the total enhancement is a combination of a CHEM enhancement of about 50 and an EM enhancement of about 3×10^2. As expected, we see that the EM enhancement from the small Ag_{20} cluster is smaller than for realistic sized nanoparticles. Experimentally the SERS spectra of adenine is dominated by a ring breathing mode around 730 cm^{-1} and a ring stretch mode at around 1330 cm^{-1}.[65] Using DFT, Giese et al.[65] assigned the mode at 1288 cm^{-1} to the experimental band at 1330 cm^{-1}, which is in good agreement with our findings because this mode is strongly enhanced in the SERS spectra. These results show that good agreement with the experimental data can be achieved by including explicitly the silver cluster in the calculations and accounting for both the CHEM and the EM enhancements. The results also support the assignment made by Giese et al.[65] that adenine absorbs through the N7 atom.

However, the strongest band at 730 cm^{-1} in the experiments is severely underestimated in our simulation of the SERS spectra as was the case in the ground state. At this point we do not know if this discrepancy is due to shortcomings of the xc-functional used in the calculations or to other effects such as adenine forming supermolecular structures on the surface. It is known that adenine forms homochiral structures when absorbed on a Cu(110) surface.[78,79] However, so far this has not been demonstrated for SERS active substrates. This is particularly interesting because SERS of DNA is generally dominated by signals from the individual bases, in particular the 730 cm^{-1} band of adenine.[80,81] It is therefore of interest to establish the intrinsic SERS properties of the individual base pairs because SERS has attracted tremendous interest for label-free DNA detection due to its unique sensitivity.[80−82]

In Figure 5 we present the simulated SEROA spectra at incident wavelengths of 514.5 and 344 nm, and the simulated SEVCD spectrum of the adenine−Ag_{20} complex. Similar to the Raman cross-sections, we attribute the enhancements at 514.5 nm to the CHEM mechanism and at 344 nm to a combination of the CHEM and EM mechanism. If we compare the SEROA spectrum of the complex at 514.5 nm (Figure 5c) with the ROA spectrum of adenine (Figure 3b), we notice that the two spectra look very different and that the intensities are around 100 times stronger for the complex. Similar to what was found for the

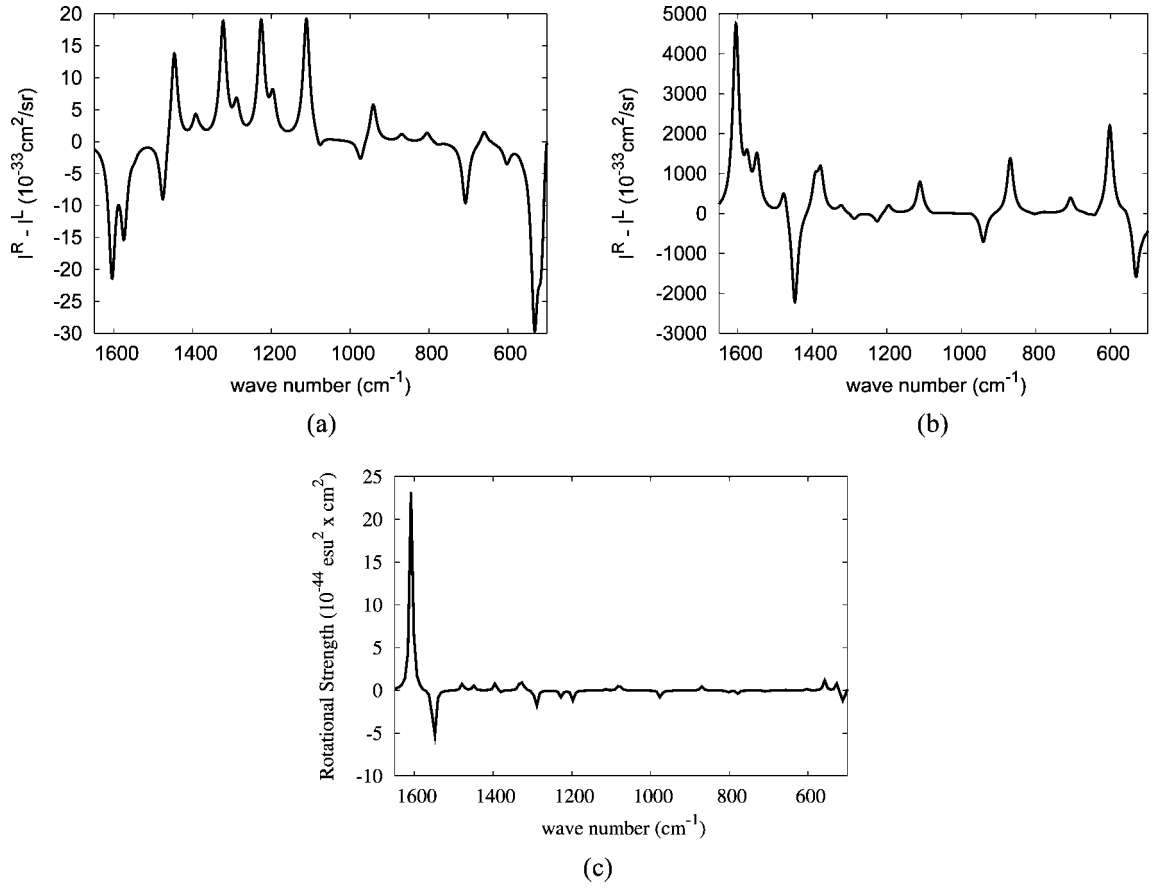

Figure 5. Simulated (a) SEROA at an incident wavelength of 514.5 nm, (b) SEROA spectra at an incident wavelength of 344 nm, and (c) SEVCD for adenine−Ag_{20}. SEROA in units of 10^{-33} cm^2/sr and SEVCD in units of 10^{-44} esu^2 × cm^2. All simulated spectra have been broadened with a Lorentzian having a full width at half-maximum (fwhm) of 20 cm^{-1}.

CHEM-enhanced SERS spectra, we see that there are more strong bands, especially in the region around 1600−1200 cm^{-1}. The average CID is found to be $\langle\Delta\rangle \sim 0.85 \times 10^{-3}$ which is slightly larger than the average CID found in the gas phase. Therefore, we see that the CHEM enhancement is larger for SEROA than for SERS scattering.

Comparing the simulated SEROA spectrum at 344 nm of the complex (Figure 5b) with the ROA spectrum of adenine (Figure 3b), we see that the enhancements are on the order of 10^4 and thus comparable with the enhancements found for Raman. The average CID is found to be $(\Delta) \sim 0.61 \times 10^{-3}$ and thus slightly less than the SERS enhancement. Although both SERS and SEROA show comparable total enhancements, the CHEM enhancement is slightly larger in SEROA than SERS. The SEROA spectrum at 344 nm is found to be very different from both the SEROA spectrum at 514.5 nm and the free adenine molecule. We see that the SEROA spectrum is dominated by a strong positive peak around 1600 cm^{-1}, a strong negative peak around 1450 cm^{-1}, and a positive-negative doublet around 600 cm^{-1}. Note that the modes that are strongly enhanced in SEROA are different from the modes enhanced in SERS. This shows that SEROA can provide different structural information than SERS and is likely to be very sensitive to the orientation of the molecule at the surface. We also see that the SEROA spectrum of adenine interacting with the metal cluster show the characteristic negative and positive peaks of ROA. Previous experimental[83] and theoretical work[30,84] has found that the resonance ROA effect is characterized by monosignate bands if the resonance is due to a single electronic state. However, deviations should be expected when more than one excited state contribute significantly to the resonance effect. This is the case in the SEROA spectrum where many states contribute to forming the strong absorption band at 344 nm.

The SEVCD spectra of adenine (Figure 5c) is dominated by a strong positive peak around 1600 cm^{-1} and a smaller negative peak at 1550 cm^{-1} with all other peaks being very weak. Comparing with the VCD spectra of the free adenine molecule, we see that the intensities of the strongest peak is enhanced by a around a factor of 20 and that the sign has changed. The enhancement in SEVCD is thus slightly lower than what is found for CHEM enhancement in SEROA. In general we find that more peaks are enhanced in SEROA than in SEVCD. Experimental evidence for SEVCD has been reported for monolayer-protected gold clusters formed from chiral adsorbates.[66−68] Here it was demonstrated[67] that the VCD spectra of small gold nanoparticles (<2 nm) covered with adsorbed *N*-isobutyrylcysteine show a mirror image relationship for particles covered with the two enantiomers. However, so far this has not been demonstrated experimentally for SEROA. Therefore, the direct comparison between theory and experiment for SEROA is likely to be successful when measurement of mirror image spectra of small enantiomers are available.[21] We believe that SEROA measurement is possible for monolayer-protected gold nanoclusters with chiral adsorbates because they show strong CD signals. Experimentally, enhanced Raman spectra of benzenethiole monolayer-protected gold nanoclusters with core diameters of ∼1.7 and ∼1.5 nm have been demonstrated. Such measurement could provide detailed insights into the induced chiroptical

properties of monolayer-protected metal cluster. To understand if SEROA is useful for studying monolayer protected metal cluster, we are currently investigating SEROA of chiral molecules interacting with a small metal cluster as a model system.

Conclusions

We presented the first simulations of the surface-enhanced Raman optical activity (SEROA) using time-dependent density functional theory (TDDFT). By employing a recently developed approach based on a short-time approximation for the Raman and ROA cross-sections, we achieved a consistent treatment of both the chemical and electromagnetic enhancements. A detailed comparison between the SERS and SEROA was presented for a model system consisting of adenine interacting with a Ag_{20} cluster. The chiroptical properties of the complex are due to the adenine−cluster interactions because both are achiral in their absorption geometry. The total enhancement was found to be on the order of 10^4 for both SEROA and SERS. However, the CHEM enhancement was found to be larger for SEROA than for SERS. The results represented here shows that SEROA can be a useful approach for studying induced chirality in small metal clusters due to the absorption of molecules.

Acknowledgment. L.J. acknowledges start-up funds from Penn State University, and support received from Research Computing and Cyberinfrastructure, a unit of Information Technology Services at Penn State University.

References and Notes

(1) Zhu, F. J.; Isaacs, N. W.; Hecht, L.; Barron, L. D. *Structure* **2005**, *13*, 1409–1419.
(2) Zhu, F. J.; Isaacs, N. W.; Hecht, L.; Tranter, G. E.; Barron, L. D. *Chirality* **2006**, *18*, 103–115.
(3) Barron, L. D. *Curr. Opin. Struct. Biol.* **2006**, *16*, 638–643.
(4) Kapitán, J.; Baumruk, V.; Kopeckú, Jr., V.; Bouř, P. *J. Phys. Chem. A* **2006**, *110*, 4689–4696.
(5) Kapitan, J.; Baumruk, V.; Bour, P. *J. Am. Chem. Soc.* **2006**, *128*, 2438–2443.
(6) Macleod, N. A.; Johannessen, C.; Hecht, L.; Barron, L. D.; Simons, J. P. *Int. J. Mass Spectrom.* **2006**, *253*, 193–200.
(7) McColl, I. H.; Blanch, E. W.; Hecht, L.; Barron, L. D. *J. Am. Chem. Soc.* **2004**, *126*, 8181–8188.
(8) McColl, I. H.; Blanch, E. W.; Gill, A. C.; Rhie, A. G. O.; Ritchie, M. A.; Hecht, L.; Nielsen, K.; Barron, L. D. *J. Am. Chem. Soc.* **2003**, *125*, 10019–10026.
(9) Syme, C. D.; Blanch, E. W.; Holt, C.; Jakes, R.; Goedert, M.; Hecht, L.; Barron, L. D. *Eur. J. Biochem.* **2002**, *269*, 148–156.
(10) Zhu, F. J.; Isaacs, N. W.; Hecht, L.; Barron, L. D. *J. Am. Chem. Soc.* **2005**, *127*, 6142–6143.
(11) Bell, A. F.; Hecht, L.; Barron, L. D. *J. Am. Chem. Soc.* **1998**, *120*, 5820–5821.
(12) Blanch, E. W.; Hecht, L.; Syme, C. D.; Volpetti, V.; Lomonossoff, G. P.; Nielsen, K.; Barron, L. D. *J. Gen. Virol.* **2002**, *83*, 2593–2600.
(13) Efrima, S. *Chem. Phys. Lett.* **1983**, *102*, 79–82.
(14) Efrima, S. *J. Chem. Phys.* **1985**, *83*, 1356–1362.
(15) Hecht, L.; Barron, L. D. *Chem. Phys. Lett.* **1994**, *225*, 525–530.
(16) Hecht, L.; Barron, L. D. *J. Mol. Struct.* **1995**, *348*, 217–220.
(17) Janesko, B. G.; Scuseria, G. E. *J. Chem. Phys.* **2006**, *125*, 124704.
(18) Abdali, S. *J. Raman Spectrosc.* **2006**, *37*, 1341–1345.
(19) Abdali, S.; Johannessen, C.; Nygaard, J.; Nørbygaard, T. *J. Phys.: Condens. Matter* **2007**, *19*, 285205.
(20) Johannessen, C.; White, P. C.; Abdali, S. *J. Phys. Chem. A* **2007**, *111*, 7771–7776.
(21) Abdali, S.; Blanch, E. W. *Chem. Soc. Rev.* **2008**, *37*, 980–992.
(22) Moskovits, M. *Rev. Mod. Phys.* **1985**, *57*, 783–826.
(23) Campion, A.; Kambhampati, P. *Chem. Soc. Rev.* **1998**, *27*, 241–250.
(24) Kneipp, K.; Kneipp, H.; Itzkan, I.; Dasari, R. R.; Feld, M. S. *Chem. Rev.* **1999**, *99*, 2957–2976.
(25) Link, S.; El-Sayed, M. A. *Annu. Rev. Phys. Chem.* **2003**, *54*, 331–366.
(26) Jensen, L.; Aikens, C. M.; Schatz, G. C. *Chem. Soc. Rev.* **2008**, *37*, 1061–1073.
(27) Bour, P. *J. Chem. Phys.* **2007**, *126*, 136101.
(28) Otto, A. Surface enhanced Raman scattering: "classical" and "chemical" origins In *Topics of Applied Physics 54, "Light Scattering in Solids"*; Cardona, M., Güntherodt, G., Eds.; Springer: New York, 1984; Vol. IV, pp 289−418.
(29) Schatz, G. C.; Van Duyne, R. P. Electromagnetic mechanism of surface enhanced spectroscopy In *Handbook of Vibrational Spectroscopy*; Chalmers, J. M., Griffiths, P. R., Eds.; John Wiley and Sons, Ltd.: New York, 2002; Vol. 1, pp 759−774.
(30) Jensen, L.; Autschbach, J.; Krykunov, M.; Schatz, G. C. *J. Chem. Phys.* **2007**, *127*, 134101.
(31) Zhao, L. L.; Jensen, L.; Schatz, G. C. *J. Am. Chem. Soc.* **2006**, *128*, 2911–2919.
(32) Zhao, L. L.; Jensen, L.; Schatz, G. C. *Nano Lett.* **2006**, *6*, 1229–1234.
(33) Jensen, L.; Zhao, L. L.; Schatz, G. C. *J. Phys. Chem. C* **2007**, *111*, 4756–4764.
(34) Barron, L. D. *Molecular Light Scattering and Optical Activity*, 2nd ed.; Cambridge University Press: New York, 2004.
(35) Barron, L. D.; Hecht, L.; McColl, I. H.; Blanch, E. W. *Mol. Phys.* **2004**, *102*, 731–744.
(36) Hug, W. Raman Optical Activity Spectroscopy In *Handbook of Vibrational Spectroscopy*; Chalmers, J. M., Griffiths, P. R., Eds.; John Wiley and Sons, Ltd.: New York, 2002; Vol. 1, pp 745−758.
(37) Schulman, J. M.; Detrano, R.; Musher, J. I. *Phys. Rev. A* **1972**, *5*, 1125–1131.
(38) Schulman, J. M.; Detrano, R. *Phys. Rev. A* **1974**, *10*, 1192–1197.
(39) Schulman, W. S.; Lee, J. M. *J. Chem. Phys.* **1981**, *74*, 4930–4935.
(40) Lee, S.-Y. *J. Chem. Phys.* **1982**, *76*, 3064–3074.
(41) Lee, S.-Y. *J. Chem. Phys.* **1983**, *78*, 723–734.
(42) Jensen, L.; Zhao, L. L.; Autschbach, J.; Schatz, G. C. *J. Chem. Phys.* **2005**, *123*, 174110.
(43) Jensen, L.; Autschbach, J.; Schatz, G. C. *J. Chem. Phys.* **2005**, *122*, 224115.
(44) Autschbach, J.; Jensen, L.; Schatz, G. C.; Tse, Y. C. E.; Krykunov, M. *J. Phys. Chem. A* **2006**, *110*, 2461–2473.
(45) Krykunov, M.; Autschbach, J. *J. Chem. Phys.* **2005**, *123*, 114103.
(46) Krykunov, M.; Autschbach, J. *J. Chem. Phys.* **2006**, *125*, 034102.
(47) Krykunov, M.; Autschbach, J. *J. Chem. Phys.* **2007**, *126*, 024101.
(48) Boyd, R. W. *Nonlinear Optics*; Academic Press: San Diego, 1992.
(49) Schatz, G. C.; Ratner, M. A. *Quantum Mechanics in Chemistry*; Dover: New York, 2002.
(50) Sue, J.; Yan, Y. J.; Mukamel, S. *J. Chem. Phys.* **1986**, *85*, 462–474.
(51) Meyers, A. B. *Annu. Rev. Phys. Chem.* **1998**, *49*, 267–295.
(52) Pedersen, T. B.; Koch, H.; Boman, L.; Sánchez de Merás, A. M. *J. Chem. Phys. Lett.* **2004**, *393*, 319–326.
(53) Baerends, E. J. et al. Amsterdam Density Functional. http://www.scm.com.
(54) te Velde, G.; Bickelhaupt, F. M.; Baerends, E. J.; Fonseca Guerra, C.; van Gisbergen, S. J. A.; Snijders, J. G.; Ziegler, T. *J. Comput. Chem.* **2001**, *22*, 931.
(55) Becke, A. D. *Phys. Rev. A* **1988**, *38*, 3098.
(56) Perdew, J. P. *Phys. Rev. B* **1986**, *33*, 8822.
(57) van Lenthe, E.; Baerends, E. J.; Snijders, J. G. *J. Chem. Phys.* **1993**, *99*, 4597–4610.
(58) van Lenthe, E.; Baerends, E. J.; Snijders, J. G. *J. Chem. Phys.* **1994**, *101*, 9783–9792.
(59) Neugebauer, J.; Hess, B. A. *J. Chem. Phys.* **2003**, *118*, 7215–7225.
(60) Doye, J. P. K.; Wales, D. J. *New J. Chem.* **1998**, *22*, 733–744.
(61) Krykunov, M.; Banerjee, A.; Ziegler, T.; Autschbach, J. *J. Chem. Phys.* **2005**, *122*, 074105.
(62) Lombardi, J. R.; Birke, R. L.; Lu, T.; Xu, J. *J. Chem. Phys.* **1986**, *84*, 4174–4180.
(63) Lombardi, J. R.; Birke, R. L. *J. Chem. Phys.* **2007**, *126*, 244709.
(64) Nicu, V.; Neugebauer, J.; Wolff, S.; Baerends, E. *Theor. Chim. Acta* **2008**, *119*, 245–263.
(65) Giese, B.; McNaughton, D. *J. Phys. Chem. B* **2002**, *106*, 101–112.
(66) Gautier, C.; Burgi, T. *Chem. Commun.* **2005**, 5393–5395.
(67) Gautier, C.; Brgi, T. *J. Am. Chem. Soc.* **2006**, *128*, 11079–11087.
(68) Bieri, M.; Gautier, C.; Burgi, T. *Phys. Chem. Chem. Phys.* **2007**, *9*, 671–685.
(69) Sponer, J.; Hobza, P. *J. Phys. Chem.* **1994**, *98*, 3161–3164.
(70) Humphrey, W.; Dalke, A.; Schulten, K. *J. Mol. Graph.* **1996**, *14*, 33–38.
(71) Zeigler, T.; Rauk, A. *Theor. Chim. Acta* **1977**, *46*, 1–10.
(72) Ziegler, T.; Rauk, A. *Inorg. Chem.* **1979**, *18*, 1558–1565.
(73) Ziegler, T.; Rauk, A. *Inorg. Chem.* **1979**, *18*, 1755–1759.
(74) Bickelhaupt, F. M.; Baerends, E. J. Kohn-Sham density functional theory: predicting and understanding chemistry In *Reviews in Computational Chemistry*; Lipkowitz, K. B., Boyud, B., Eds.; Wiley-VCH: New York, 2000; Vol. 15, pp 1−86.
(75) Schaaff, T.; Whetten, R. *J. Phys. Chem. B* **2000**, *104*, 2630–2641.

(76) Goldsmith, M.-R.; George, C. B.; Zuber, G.; Naaman, R.; Waldeck, D. H.; Wipf, P.; Beratan, D. N. *Phys. Chem. Chem. Phys.* **2006**, *8*, 63–67.
(77) Jimenez-Hoyos, C. A.; Janesko, B. G.; Scuseria, G. E. *Phys. Chem. Chem. Phys.* **2008**, *10*, 6621–6629.
(78) Chen, Q.; Frankel, D. J.; Richardson, N. V. *Langmuir* **2002**, *18*, 3219–3225.
(79) Chen, Q.; Richardson, N. V. *Nat. Mater.* **2003**, *2*, 324–328.
(80) Bell, S. E. J.; Sirimuthu, N. M. S. *J. Am. Chem. Soc.* **2006**, *128*, 15580–15581.
(81) Barhoumi, A.; Zhang, D.; Tam, F.; Halas, N. J. *J. Am. Chem. Soc.* **2008**, *130*, 5523–5529.
(82) Kneipp, K.; Kneipp, H.; Kartha, V. B.; Manoharan, R.; Deinum, G.; Itzkan, I.; Dasari, R. R.; Feld, M. S. *Phys. Rev. E* **1998**, *57*, R6284.
(83) Vargek, M.; Freedman, T. B.; Lee, E.; Nafie, L. A. *Chem. Phys. Lett.* **1998**, *287*, 359–364.
(84) Nafie, L. A. *Chem. Phys.* **1996**, *205*, 309–322.

JP811084X